Eng. Sci., 2021, **17**, 176–184

Engineered Science

DOI: https://dx.doi.org/10.30919/es8d534

Solvothermal Synthesis of Anatase TiO_2 for the Detoxification of Methyl Orange Dye with Improved Photodegradation Efficiency

Rekha B. Rajput, Shweta N. Jamble and Rohidas B. Kale*

Abstract

TiO_2 nanomaterials are one of the most significant nanomaterials among the various metal oxide semiconductors family. The TiO_2 nanomaterials exhibit good chemical and biological stability, nontoxicity, high degradation efficiency, and good permeability. Hence TiO_2 nanomaterials are used for the photodegradation of organic pollutants, toxic dyes, and other forms of environmental contaminants. In this work, the anatase TiO_2 nanomaterials were efficiently synthesized via a solvothermal method, with crystallite sizes ranging from 6.8-7.1 nm. The morphological observations revealed that various shapes and sizes of microparticles were formed by the agglomeration of nanoparticles. The energy-dispersive X-ray analysis confirmed that the titanium-oxygen stoichiometric ratio was approximately 1:2. The energy band gap of TiO_2 nanomaterials was in the range of 3.02-3.12 eV. The photoluminescence study showed that anatase TiO_2 nanomaterial (T2) is ascribed to the self-trapped excitons, surface states, and oxygen vacancies. The T2 sample has shown red-shifted with a high surface area (183.17 m^2/g) and large pore size (4.58 nm), which helps to achieve photocatalytic degradation of methyl orange up to 90% within 30 min of mercury light irradiation. The scavenger test indicated that h^+ radicals are important reactive species in the photodegradation process.

Keywords: Titania; Solvothermal Synthesis; Hydroxyl radicals; Organic dyes; Water treatment.
Received: 23 June 2021; Revised: 15 September 2021; Accepted: 17 September 2021.
Article type: Research article.

1. Introduction

In the last few decades, many industries such as textiles, leather, printing, and ink industries are using toxic dyes to color their material and release wastewater into various aquatic streams.[1,2] This dye-containing wastewater is very harmful to aquatic life and ecology.[3] Many dyes cause skin irritation, allergic dermatitis, and carcinogenic and mutagenic issues.[4,5] These toxic dyes are not only harmful to aquatic animals but also badly affect human health. Moreover, these pollutants are difficult to decompose into less hazardous by-products under natural circumstances.[6] For the detoxification of such organic pollutants, semiconductor nanomaterials can be used as a photocatalyst that acts as a clean energy source.[7] The photocatalysis activity has attracted more attention due to its simplicity, high efficiency, cost-effectiveness, non-toxicity, good permeability, and less secondary pollution.[8-10]

In recent years, TiO_2 nanomaterial has been widely studied in several industries due to its various applications in water splitting,[11] mineralization of organic pollutants,[12,13] dye-sensitized solar cells[14] and gas sensors,[15] due to its special electronic and optical properties, high physicochemical stability, low cost, corrosion resistance and abundance in nature.[16,17] The TiO_2 nanomaterial naturally occurs in three major crystal structures such as polymorph anatase (tetragonal), rutile (tetragonal), and brookite (orthorhombic), with exhibited energy band gaps 3.2, 3.0 and 3.2 eV, respectively.[18,19] The primary application of TiO_2 nanomaterial is widely used as an additive into a white pigment in paints, cosmetics, toothpaste, food coloring, and polymers.[20] For the synthesis of TiO_2 nanomaterials, various techniques have been developed, such as hydrothermal, solvothermal, electrochemical deposition, chemical bath deposition, sol-gel, co-precipitation, chemical vapor deposition, sonochemical method, atomic layer deposition, and microwave-assisted hydrothermal method.[21-30] Among them, the solvothermal method has outstanding advantages like high purity material, better-controlled size/shape, low-temperature processing, reduce manufacturing cost, less

Department of Physics, The Institute of Science, Madam Cama Road, Mumbai, India.
**Email:* rb.kale.phy@gmail.com (R.B. Kale)

hazardous and easy-to-change experimental parameters such as reaction temperature, time, different surfactants, solvents, and various precursors.[31,32] Zhao *et al*. reported the fabrication of anatase TiO_2 sheets using a simple hydrothermal method. They explained that the photocatalyst prepared at 180 °C exhibited the highest degradation efficiency of methyl orange (MO) up to 95% within 120 min of UV irradiation, as depicted in Table 1.[33] Wu *et al*. and co-authors have reported the production of carbon-doped TiO_2 powder by the calcination-assisted solvothermal method that shows the photodegradation of MO up to 98% within 120 min of visible light irradiation.[34] Thapa *et al*. synthesized anatase TiO_2 nanoparticles via a hydrothermal route and further used them for the detoxification of MO within 25 min under UV irradiation.[35] Xue *et al*. reported the synthesis of hollow TiO_2 nanostructures employing by hydrothermal method using $TiCl_3$ as a starting precursor. They reported the complete degradation of MO within 80 min of UV irradiation.[36]

In this study, TiO_2 nanomaterials were easily synthesized by the simple and effective solvothermal method, and studied their structural, morphological, and optical properties were. The obtained TiO_2 nanomaterials (T2 sample) showed enhanced photocatalytic performance for methyl orange dye (MO) degradation under mercury light irradiation. Also, we have explained the photocatalytic mechanism. Finally, the findings of the experiment were thoroughly discussed.

2. Experimental

2.1 Chemicals and materials

Analytical reagent grade (AR) titanium isopropoxide (TTIP), 2-propanol, sodium hydroxide, acetic acid, and MO dye purchased from S. D Fine Chem. Ltd., Mumbai, and further used without purification.

2.2 Photocatalyst preparation

In a typical synthesis process, 0.2 M titanium isopropoxide and 0.25 M sodium hydroxide (NaOH) were simultaneously added to the mixture of distilled water and 2-propanol solution (1:2 ratio) under vigorous stirring. The resultant mixture was kept in constant stirring for the next 15 min. After mixing both solutions, 5 mL of acetic acid was added dropwise into the mixture. Then the above solution was transferred in a Teflon-lined stainless-steel autoclave. Afterward, an autoclave was kept in a hot air oven at 140, 160, and 180 °C temperature for 5 h and air-cooled to ambient temperature. The final product was collected, washed several times with distilled water, dried at 100 °C for 5 h, and used for further characterization. The TiO_2 samples synthesized at 140, 160, and 180 °C were labeled as T1, T2, and T3, respectively.

2.3 Characterizations

The crystallographic phases of synthesized TiO_2 nanomaterials were carried by using Proto manufactured AXRD diffractometer (XRD) equipped with CuK_α radiation (λ = 1.54 Å) at a scan rate of 5° min^{-1} with the 2θ range from 20 to 70°. To study surface morphology and chemical composition, a scanning electron microscope (SEM, JEOL, JSM-IT300) equipped with energy-dispersive X-ray analysis (EDS, Oxford Instrument) was used. The absorbance spectra were obtained using a UV-vis spectrophotometer (PerkinElmer, Lambda 750). A fluorescence spectrophotometer (PerkinElmer, LS-55) was employed to obtain the photoluminescence (PL) spectra of a synthesized sample at room temperature. The high-resolution transmission electron microscopy (HRTEM) images were taken using FEG-TEM (JEM 2100F) instrument with an operating voltage of 200 kV. The specific surface areas and pore diameter of the TiO_2 samples were obtained by nitrogen adsorption using a Micromeritics ASAP 020 Surface Area and Porosity Analyser.

2.4 Photocatalytic activity test

The photocatalytic performance of the TiO_2 nanomaterials was monitored for the detoxification of MO under 125 W mercury light irradiation (PHILIPS 125 W E27). Here, 50 mg of TiO_2 nanomaterials were suspended in 50 mL of 10 mg/L MO dye aqueous solution. To achieve adsorption-desorption equilibrium, the solution was constantly stirred in the dark for 30 min. During irradiation, an aliquot of 4-5 mL was withdrawn from the suspension using a UV-vis spectrophotometer; the spectrum was analyzed in the wavelength range 350-650 nm after being centrifuged. Further, the degradation percentage of MO was calculated from the equation as follows.

$$D\% = \left(\frac{C_o - C_t}{C_o}\right) \times 100 \quad (1)$$

where C_0 is the MO concentration at time t = 0 and C_t is the MO concentration at time t where t is irradiation time.

3. Results and discussion

3.1 Structural analysis

Figure 1 shows the X-ray diffraction pattern of solvothermal synthesized TiO_2 nanomaterials at 140, 160, and 180 °C for 5 h. The peaks at '2θ' values are 25.44, 38.04, 48.15, 54.29, 62.89, and 69.04° and their hkl planes could be indexed to the (101), (004), (200), (105), (204) and (116) crystalline planes. The diffraction pattern revealed that the prepared TiO_2 nanomaterials could be indexed to the anatase phase with the tetragonal crystal structure (JCPDS NO. 21-1272), with no additional impurity peaks observed.

The Debey Scherrer equation was used to find the average crystallite size of the synthesized TiO_2 nanomaterials, which is given below:[22]

$$D = \frac{(0.9\lambda)}{(\beta Cos\theta)} \quad (2)$$

where D is the average crystallite size, λ is used X-ray wavelength (0.154 nm), β is the full width at half maximum (FWHM) and θ is the diffraction angle. The crystallite size of synthesized TiO_2 nanomaterials T1, T2, and T3 was found to be 5.7, 6.8, and 7.3 nm from the prominent diffraction peak. This finding suggests that as the temperature rises, the crystallite size of the TiO_2 nanomaterials increases.

3.2 Elemental composition analysis

Figure S1(a) reveals the elemental composition and purity of the T2 sample estimated using the EDS technique. The strong titanium (Ti) and oxygen (O) peaks were observed without any impurity, confirming the synthesized TiO_2. The Ti and O were found to have average atomic percentages of 27.78 and 72.22, respectively. The result depicts the synthesized TiO_2 nanomaterial is in a good stoichiometric ratio. Also, by color mapping analysis, Figs. S1(b-d) displays the existence of all expected elements Ti and O in the T2 sample.

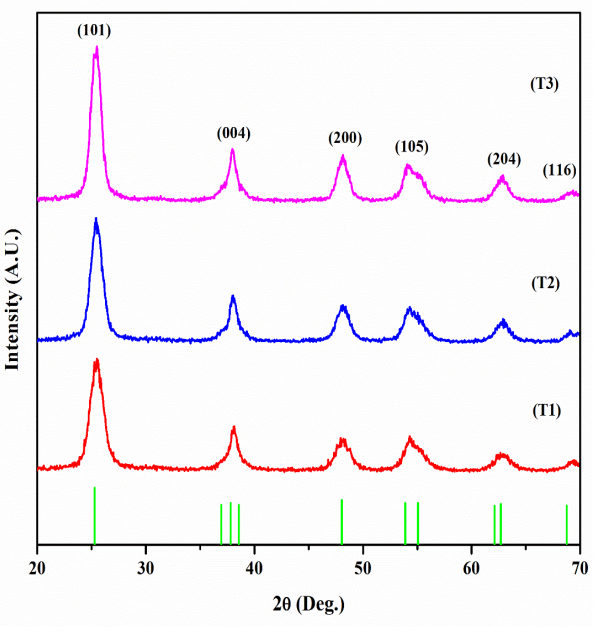

Fig. 1 XRD pattern of the synthesized TiO_2 nanomaterials T1, T2, and T3 were synthesized at 140, 160, and 180 °C, respectively.

3.3 Morphological study

Figures S2(a-c) exhibits the SEM morphology of the as-synthesized TiO_2 nanomaterials T1, T2, and T3, respectively. The SEM images reveal the stone-like microparticles with various shapes and sizes with an average diameter of about 0.1-3 µm, as shown in Fig. S2(d). HRTEM images of the T2 sample with average microparticle diameters of approximately 0.2-0.3 µm are shown in Fig. 2(a), consistent with the SEM image. These microparticles consist of a small aggregation of TiO_2 nanoparticles with an average diameter of 2-7 nm, as shown in Fig. 2(d).

Figure 2(e) depicts the HRTEM image of the T2 sample that reveals the lattice spacing with a distance of 0.351 nm, which corresponds to the (101) plane that is well consistent with the XRD result. Fig. 2(f) depicts the selected area electron diffraction (SAED) pattern of the T2 sample. It shows the patterns of concentric rings with intermittent dots, indicating the polycrystalline nature of TiO_2.

3.4 UV-vis analysis

The optical energy band gap (E_g) of synthesized TiO_2 nanomaterials T1, T2 and T3 can be determined using Tauc's relation as shown below:[35]

$$(\alpha hv) = A(hv - Eg)^n \quad (3)$$

where A is constant, α is the absorption coefficient, *hv* is photon energy and E_g is the band gap of the synthesized materials. The exponent *n* is equal to ½ or 2 for direct or indirect band gap transition materials. Fig. 3 shows the plot of $(\alpha hv)^{1/2}$ versus *hv* of the TiO_2 nanomaterials and the inset depicts the corresponding absorption spectra of the synthesized samples. The extrapolation of the linear part of the plot to the energy axis (α = 0) gives the energy band gap value of the synthesized TiO_2 nanomaterials T1, T2 and T3 are around 3.08, 3.02, and 3.12 eV, respectively.

3.5 BET analysis

N_2 adsorption-desorption analysis was used to examine the specific surface area and pore size of the TiO_2 sample synthesized at 140, 160, and 180 °C. Fig. S3 depicts the N_2 adsorption-desorption isotherm of T1, T2, and T3 samples, respectively. According to IUPAC, the isotherm represented a type IV isotherm with H_2 hysteresis loops. The hysteresis loops in the 0.4–1.0 (P/P0) range belonged to H_2 hysteresis loops, indicating that the nanostructures were mesoporous. The BET and BJH methods were used to determine the surface area, pore size, and pore volume of the T1, T2, and T3 samples, as shown in Table 2. The T1, T2, and T3 samples' BET surface areas were 205.67, 183.17, and 169.73 m^2g^{-1}, respectively. In addition, using the template-free solvothermal process, high-surface-area TiO_2 samples were obtained. In general, a large pore volume and a high specific surface area can provide more contact sites for the reactant molecule, which is beneficial to increase photocatalytic activity.[37]

3.6 Photoluminescence study

Photoluminescence spectra are a vital characterization tool to study the generation-recombination of e^-/h^+ pairs, trapping, immigration, and various forms of defects present in the material.

Figure 4 shows the PL emission spectra of the as-synthesized TiO_2 nanomaterial (160 °C) exhibit emission peaks at 401, 423, 446, 463, and 487 nm with an excitation wavelength of 250 nm. The emission peak centered at 401 and 423 nm was attributed to excitonic emission to the near band edge emission of TiO_2.[38,39] The emission band at 446 nm was assigned to the oxygen vacancy.[40] The emission near 463 nm was shown as a result of the e^- transition between the donor and deep acceptor levels.[39] Also, due to the surface state, the emission band at 487 nm was seen.[41]

3.7 Photocatalytic Activities

Figure 5(a) displays the photodegradation spectra of MO in the wavelength range of 200–600 nm over time using a T2 catalyst. These spectra explained the absorption peak intensity at 465 nm continuously decreases with an increase in irradiation time and around 90% MO was degraded within 30 min. The photodegradation of MO dye was compared to that of previously recorded TiO_2 nanomaterials in Table 1.

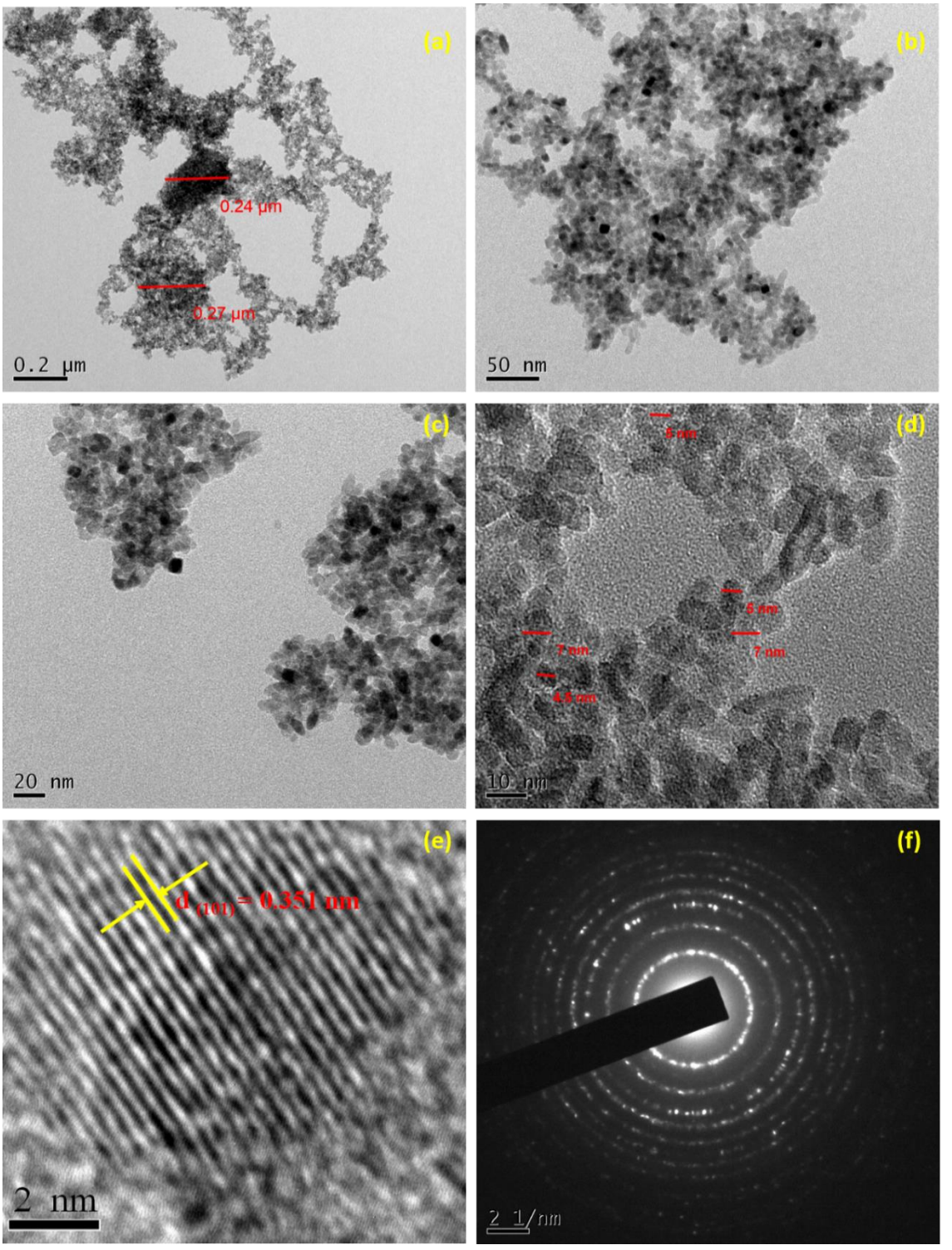

Fig. 2 (a-d) TEM images of different magnifications, (e) HR-TEM image, and (f) SAED pattern with lattice fringes of T2 sample.

Figure 5(b) shows the plot of C_t/C_o versus time (t) under the mercury light irradiation of the TiO_2 nanomaterials. The rate constant of MO photodegradation was studied by using pseudo-first-order kinetics which can be expressed as a given equation,[42]

$$\ln\left(\frac{C_0}{C_t}\right) = kt \quad (4)$$

where C_o is the dye concentration at time t = 0 min, C_t is the dye concentration at time t, t is irradiation time and k is the rate constant.

The MO degradation rate constant of the T1, T2, and T3 samples were determined using the plot of ln (C_0/C_t) versus irradiation time, as shown in Fig. 5(c). From the plot, the rate constant (k) was measured to be 61.4×10^{-3}, 71.0×10^{-3}, $48.0 \times 10^{-3,}$ and 9×10^{-4} $min^{-1,}$ and the linear regression correlation coefficient R^2 was calculated to be 0.9934, 0.9899, 0.9966 and 0.9439 of T1, T2, T3, and blank sample, respectively. Also, the chemical oxygen demand (COD) of the degraded MO dye

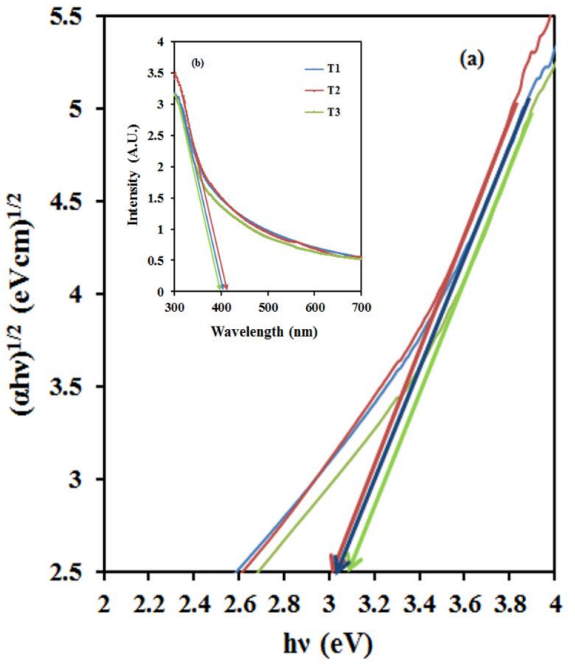

Fig. 3 Plot of $(\alpha h\nu)^{1/2}$ versus hν of the TiO_2 nanomaterials T1, T2, and T3. Inset: corresponding UV absorbance spectra.

the solution was investigated based on an open reflux titrimetric method using a spectral COD digestor. The COD of MO dye was found to be reduced within 30 min from 08 to 02 mg/L. In addition, the obtained T2 photocatalyst exhibited 75% of the total efficiency of COD removal, suggesting that the T2 photocatalyst has a higher mineralization ability.

The photocatalytic performance is primarily determined by the crystal structure, crystallite size, light absorbance ability, large surface area, and also pore size.[43] In the current study, the TiO_2 nanomaterial synthesized at 160 °C demonstrated the highest photodegradation efficiency compared to other samples. Since it has a wide surface area and large pore size, the adsorption property improves.[44] These findings show that the morphology, crystallite size, surface area, and pore size play an important role in the photocatalytic degradation of MO.

3.8 Effect of variation of MO dye and catalyst concentration on photocatalytic activity

The effect of variation in the concentration of dye was studied by keeping the amount of T2 catalyst (50 mg/L) constant. The degradation efficiency decreases as the initial MO concentration increases, as shown in Fig. 6(a). The 5 ppm

Table 1. Comparison table of degradation of methyl orange dye from TiO_2 nanoparticles.

Sr. No.	Materials	Synthesis method used	Experimental conditions	Light source	Degradation time (min)	Percentage (%)	Reference
1	TiO_2 sheets	Hydrothermal (180 °C / 12 h)	P: 50 mL, 10 mg/L C: 100 mg	UV light irradiation (300 W)	120 min	95%	[33]
2	Carbon doped TiO_2	Solvothermal (190 °C / 2 h calcined at 265 °C)	P: 50 mL, 15 mg/L C: 50 mg	Simulated solar light (300 W)	120 min	98%	[34]
3	TiO_2 nanoparticles	Hydrothermal (150 °C / 18 h)	P: 100 mL, 10^{-5} M C: 30 mg	UV light (40 W)	25 min	98%	[35]
4	Hollow TiO_2 nanoparticles	Hydrothermal (180 °C / 12 h)	P: 50 mL, 10 mg/L C: 50 mg	High-pressure Hg lamp (300 W)	80 min	99%	[36]
5	TiO_2 nanorods	Hydrothermal (180 °C / 24 h)	P: 100 mL, 10 ppm C: 50 mg	Mercury lamp (intensity is ~650 lux)	150 min	51%	[45]
6	TiO_2 nanobelts	Hydrothermal (180 °C / 10 h calcined at 550 °C)	P: 100 mL, 3×10^{-5} mol/L C: 200 mg	Sunlight (intensity 1.15 × 10^5 lx)	60 min	93%	[46]
7	TiO_2@Ag NRs	Solvothermal (200 °C / 24 h)	P: 200 mL, 20 mg/L C: 20 mg	Xe lamp (1000 W)	150 min	98%	[47]
8	Our data	Solvothermal (160 °C / 5 h)	P: 50 mL, 10 mg/L C: 50 mg	Mercury lamp (125 W)	30 min	90%	

Table 2. Nitrogen adsorption-desorption studies for TiO_2 nanomaterials.

TiO_2 photocatalyst	Crystalite size (nm)	Band gap energy (eV)	S_{BET} (m^2g^{-1})	Pore volume (cm^3g^{-1})	Pore size (nm)
T1	5.78	3.08	205.67	0.19	3.78
T2	6.80	3.02	183.17	0.21	4.58
T3	7.34	3.12	169.73	0.23	5.46

MO dye achieved up to 94% degradation efficiency within 20 min of irradiation, while the concentration of 10 ppm and 15 ppm of MO exhibited 90 and 32% degradation efficiency within 30 min. Herein, at a higher initial concentration, MO dye blocked the active catalytic surface sites in the solution, resulting in decreasing photodegradation efficiency.

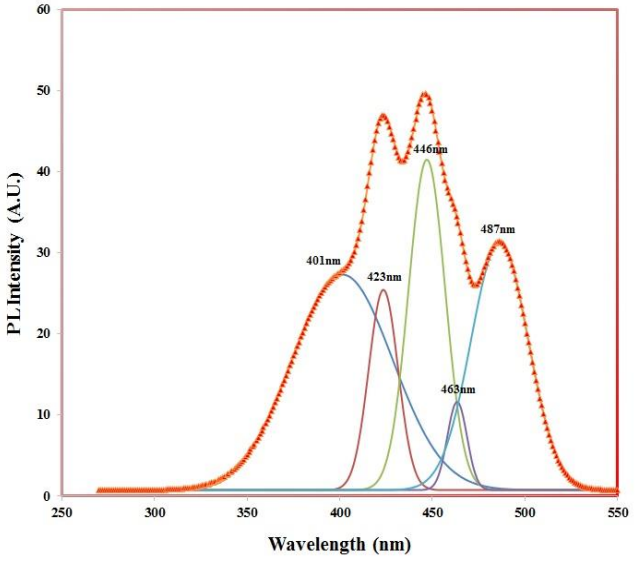

Fig. 4 Room temperature photoluminescence spectra with Gaussian fitting of the T2 sample.

The effect of catalyst variation (20, 50, and 80 mg/L) on the MO dye degradation over the TiO_2 photocatalyst (T2) was shown in Fig. 6(b). With increasing catalyst loading, it is observed that MO degradation efficiency has been improved. The 80 mg/L TiO_2 catalysts were shown > 98% degradation within 20 min, whereas 50 and 20 mg/L catalysts were shown 90 and 64% degradation within 30 min, respectively. Notably, the improvement in degradation efficiency at the highest photocatalyst quantity is primarily due to the rise in the number of active sites on the TiO_2 catalyst surface.

3.9 Scavenger test

The role of various active species in the photodegradation of MO dye is investigated using radical trapping experiments. In this method, three active species scavengers ethylenediaminetetraacetic acid tetrasodium (10 mM), isopropyl alcohol (1 mL), and L-ascorbic acid (10 mM) were used in the photocatalytic process, which are effective scavengers for the h^+, $OH^\bullet$ and $^\cdot O_2^-$ radicals, respectively. Fig. 7 depicts that after the addition of EDTA, which functions as an h^+ scavenger, photodegradation efficiency (~ 1-2%) was significantly suppressed. However, when IPA and L-ascorbic acid were added to the degradation process, there was a slight change in photodegradation efficiency than without the scavenger. The obtained results revealed that in the MO degradation process, h^+ radicals play a key role and act as major active species, whereas $OH^\bullet$ and $^\cdot O_2^-$ radicals exhibited minor active species.

3.10 Stability tests of the TiO_2 nanomaterial

Figure 8 shows the recycling test for the decomposition of 10 ppm MO dye under the same experimental conditions to determine the photostability of the TiO_2 nanomaterial (T2 sample) synthesized at 160 ºC. After the first cycle, the utilized TiO_2 photocatalyst was centrifuged, thoroughly washed with distilled water, and dried at 80 °C for 5-6 h. After three consecutive cycles, the TiO_2 photocatalyst has a significantly lower degradation efficiency (76%) than the initial degradation efficiency (90%) within 30 min of irradiation. The reduction in photocatalytic efficiency was due to the loss in catalyst recollection at the end of each cycle.

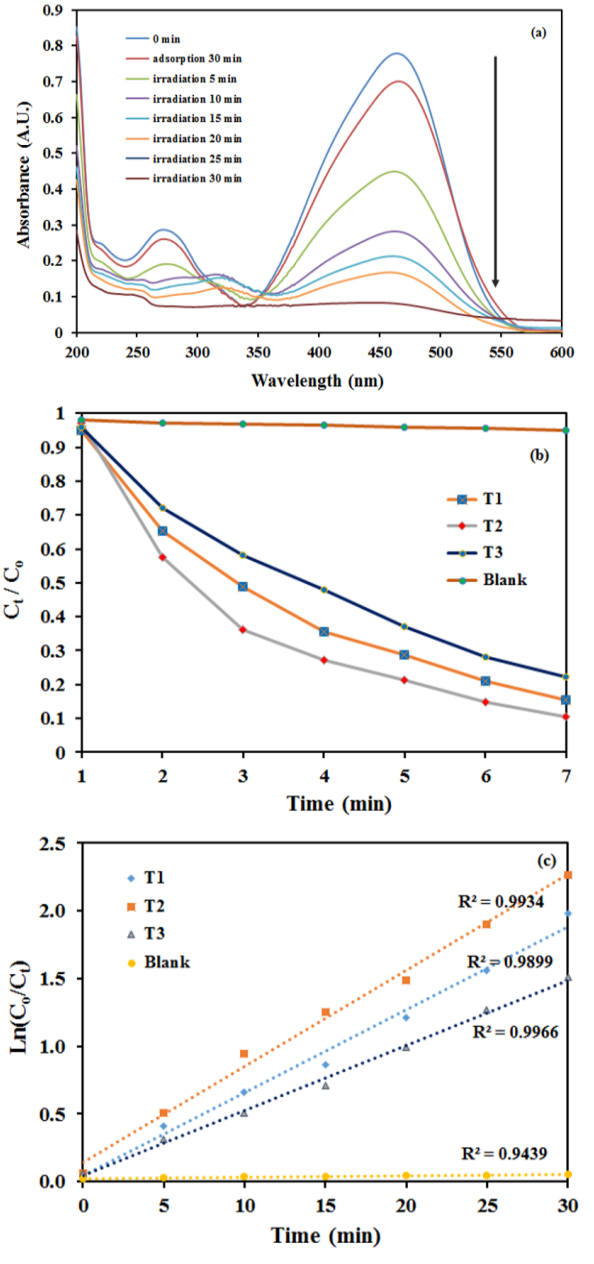

Fig. 5 (a) UV–visible spectra of MO solution in the presence of T2 sample under mercury light irradiation at different intervals, (b) Photodegradation of MO dye in the presence of T1, T2, and T3 sample, and (c) Linear plot of $ln(C_o/C_t)$ vs time over different samples.

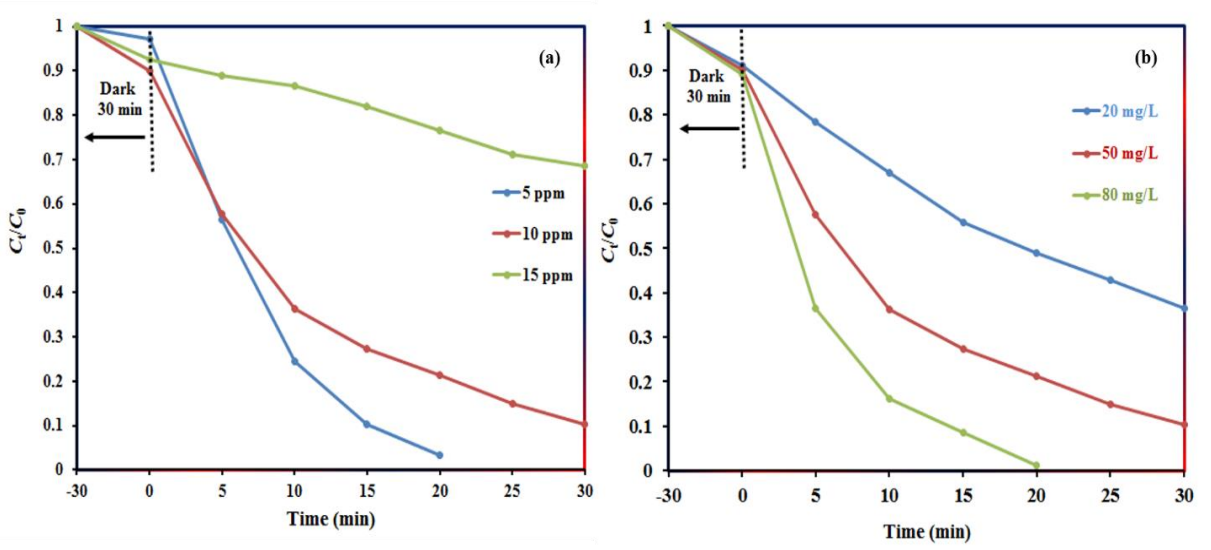

Fig. 6 (a) Effect of variation of MO dye concentration on photocatalytic activity of T2 sample and (b) Effect of variation of T2 catalyst on the photodegradation of MO dye (10 ppm).

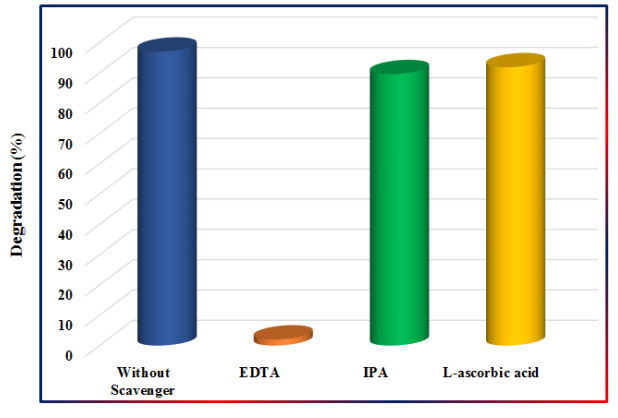

Fig. 7 Radical trapping experiment for the photodegradation of MO dye over the T2 sample.

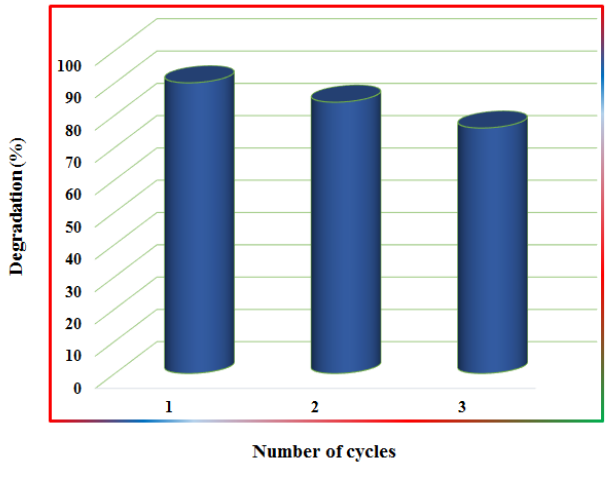

Fig. 8 Stability test of the T2 up to three cycles for the degradation of MO dye.

3.11 Photocatalytic mechanism

The photodegradation mechanism of MO dye by using TiO_2 nanomaterial was depicted in Fig. 9. When the UV-vis light falls on TiO_2 nanomaterial and if its energy is equal to or greater than the energy band gap of TiO_2 nanomaterial, then the e^-/h^+ pair was generated. Then electrons (e^-) are excited and undergo the transition from the valance band to the conduction band by leaving holes (h^+) in the valance band, which latterly diffuses near the catalyst surface. These photogenerated holes on the catalyst surface react with water and hydroxyl group (OH^-) to produce hydroxyl ($OH^\bullet$) radicals. Similarly, the photogenerated electron (e^-) on the catalyst surface reacts with dissolved oxygen to form superoxide anions. These hydroxyl radicals and superoxide anions were attached to the intermediate products in the oxidative reaction leading to the detoxification of harmful organic pollutants. The following equations explain the photocatalytic mechanism:[42]

$$TiO_2 + h\nu \rightarrow h^+_{(VB)} + e^-_{(CB)} \quad (5)$$

$$h^+_{(VB)} + H_2O \rightarrow OH^\bullet + H^+ \quad (6)$$

$$h^+_{(VB)} + OH^- \rightarrow OH^\bullet \quad (7)$$

$$e^-_{(CB)} + O_2 \rightarrow O_2^{\bullet-} \quad (8)$$

$$O_2^{\bullet-} + H^+ \rightarrow HO_2^\bullet \quad (9)$$

$$2OH^\bullet \rightarrow H_2O_2 \quad (10)$$

$$H_2O_2 + e^-_{(CB)} \rightarrow OH^\bullet + OH^- \quad (11)$$

$$OH^\bullet + O_2^{\bullet-} + \text{Dyes} \rightarrow \text{Degradation product} + H_2O + CO_2 \quad (12)$$

4. Conclusions

In summary, the solvothermal method is used to synthesize nanometric TiO_2 with the anatase crystal structure. The XRD pattern confirmed the anatase crystalline phase with a crystallite size of 6.8–7.1 nm. From the UV-vis absorption plot, the energy band gap of the TiO_2 nanomaterials is found to be 3.02-3.12 eV. The SEM observation reveals stone-like microparticles of various shapes and sizes. The HRTEM observation reveals that the microparticles are formed by the agglomeration of nanoparticles. The EDS spectrum confirms the presence of Ti and O elements and no other impurity peaks

are detected. The synthesized TiO_2 nanomaterial (T2) is used as a photocatalyst and the maximum degradation efficiency of MO is observed to be 98 and 90% for 80 and 50 mg catalyst concentration within 20 and 30 min of irradiation, respectively. The photodegradation of MO over (1 g/L) T2 catalysts achieved a COD removal efficiency of around 75%. The findings reveal that the photodegradation efficiency of MO was influenced by the quantity of MO and photocatalyst concentration. The scavenger test shows that h^+ radicals are essential reactive species involved in MO degradation. Overall, the results depict that the synthesized TiO_2 samples have the potential for color detoxification and the treatment of polluted water.

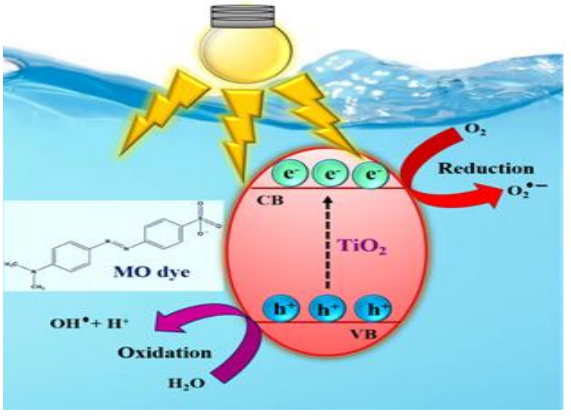

Fig. 9 Schematic diagram of the photocatalytic degradation mechanism of MO dye.

Acknowledgments

The authors are thankful to the Department of Science and Technology, India, under the DST-FIST (SR/FST/ PSI-173/2012) program. We are thankful to SAIF, IIT Bombay for HRTEM characterization. We thank Dr. Deepa Khushalani, Tata Institute of Fundamental Research, Mumbai, for BET characterization. A special thanks to the WOMEN GRADUATES UNION for providing scholarships to support and encourage research work.

Conflict of interest

There are no conflicts to declare.

Supporting information

Applicable.

References

[1] L. Ayed, A. Mahdhi, A. Cheref, A. Bakhrouf, *Desalination*, 2011, **274**, 272-277, doi: 10.1016/j.desal.2011.02.024.

[2] R. Khayyam Nekouei, F. Pahlevani, M. Mayyas, S. Maroufi, V. Sahajwalla, *Journal of Environmental Chemical Engineering*, 2019, **7**, 103133, doi: 10.1016/j.jece.2019.103133.

[3] N. S. Alharbi, B. Hu, T. Hayat, S. O. Rabah, A. Alsaedi, L. Zhuang, X. Wang, *Frontiers of Chemical Science and Engineering*, 2020, **14**, 1124-1135, doi: 10.1007/s11705-020-1923-z.

[4] M. Danish, T. Ahmad, W. N. A. W. Nadhari, M. Ahmad, W. Ahmad Khanday, Z. Lou, P. Zhou, *Applied Water Science*, 2018, **8**, 9, doi: 10.1007/s13201-018-0644-7.

[5] A. M. Al-Hamdi, U. Rinner, M. Sillanpää, *Process Safety and Environmental Protection*, 2017, **107**, 190-205, doi: 10.1016/j.psep.2017.01.022.

[6] Z. Chen, S. Zhang, Y. Liu, N. S. Alharbi, S. O. Rabah, S. Wang, X. Wang, *Science of the Total Environment*, 2020, **731**, 139054, doi: 10.1016/j.scitotenv.2020.139054.

[7] S. P. Kim, M. Y. Choi, H. C. Choi, *Materials Research Bulletin*, 2016, **74**, 85-89, doi: 10.1016/j.materresbull.2015.10.024.

[8] M. Hao, M. Qiu, H. Yang, B. Hu, X. Wang, *Science of the Total Environment*, 2021, **760**, 143333, doi: 10.1016/j.scitotenv.2020.143333.

[9] X. Liu, R. Ma, L. Zhuang, B. Hu, J. Chen, X. Liu, X. Wang, *Critical Reviews in Environmental Science and Technology*, 2021, **51**, 751-790, doi: 10.1080/10643389.2020.1734433.

[10] S. Zhang, B. Li, X. Wang, G. Zhao, B. Hu, Z. Lu, T. Wen, J. Chen, X. Wang, *Chemical Engineering Journal*, 2020, **390**, 124642, doi: 10.1016/j.cej.2020.124642.

[11] A. Kudo, Y. Miseki, *Chemical Society Reviews*, 2009, **38**, 253-278, doi: 10.1039/B800489G.

[12] S. V. Kite, D. J. Sathe, A. N. Kadam, S. S. Chavan, K. M. Garadkar, *Research on Chemical Intermediates*, 2020, **46**, 1255-1282, doi: 10.1007/s11164-019-04032-7.

[13] J. Saien, H. Nejati, *Journal of hazardous materials*, 2007, **148**, 491-495, doi: 10.1016/j.jhazmat.2007.03.001.

[14] J. P. Sawant, R. B. Kale, *Materials Letters*, 2020, **265**, 127407, doi: 10.1016/j.matlet.2020.127407.

[15] Z. Li, Z. Yao, A. Ali Haidry, T. Plecenik, L. Xie, L. Sun, Q. Fatima, *International Journal of Hydrogen Energy*, 2018, **43**, 21114-21132, doi: 10.1016/j.ijhydene.2018.09.051.

[16] A. Y. Zhang, T. Lin, Y. Y. He, Y. X. Mou, *Journal of Hazardous Materials*, 2016, **311**, 81-90, doi: 10.1016/j.jhazmat.2016.02.071.

[17] P. Chetri, P. Basyach, A. Choudhury, *Chemical Physics*, 2014, **434**, 1-10, doi: 10.1016/j.chemphys.2014.02.007.

[18] D. Dambournet, I. Belharouak, K. Amine, *Chemistry of Materials*, 2010, **22**, 1173-1179, doi: 10.1021/cm902613h.

[19] X. Chen, A. Selloni, *Chemical Reviews*, 2014, **114**, 9281-9282, doi: 10.1021/cr500422r.

[20] S. Ghosh, A. P. Das, *Toxicological & Environmental Chemistry*, 2015, **97**, 491-514, doi: 10.1080/02772248.2015.1052204.

[21] A. Kumar, G. Pandey, *American Journal of Nano Research and Applications*, 2018, **6**, 1-10, doi: 10.11648/j.nano.20180601.11.

[22] R. Bargougui, A. Oueslati, G. Schmerber, C. Ulhaq-Bouillet, S. Colis, F. Hlel, S. Ammar, A. Dinia, *Journal of Materials Science: Materials in Electronics*, 2014, **25**, 2066-2071, doi: 10.1007/s10854-014-1841-2.

[23] Y. Tu, L. Tang, M. Zheng, J. Huo, J. Wu, J. Lin, M. Huang, *Journal of Alloys and Compounds*, 2017, **694**, 1083-1088, doi: 10.1016/j.jallcom.2016.10.145.

[24] A. H. Mayabadi, V. S. Waman, M. M. Kamble, S. S. Ghosh,

B. B. Gabhale, S. R. Rondiya, A. V. Rokade, S. S. Khadtare, V. G. Sathe, H. M. Pathan, S. W. Gosavi, S. R. Jadkar, *Journal of Physics and Chemistry of Solids*, 2014, **75**, 182-187, doi: 10.1016/j.jpcs.2013.09.008.
[25] S. J. Ho, C. W. Yeh, R. V. Kumar, H. S. Chen, *Materials & Design*, 2017, **115**, 332-338, doi: 10.1016/j.matdes.2016.11.033.
[26] T. Ueda, S. Sado, K. Ueda, T. Narushima, *Materials Letters*, 2016, **185**, 290-294, doi: 10.1016/j.matlet.2016.08.066.
[27] Z. Yu, X. Qu, W. Yang, J. Peng, Z. Xu, *Journal of Alloys and Compounds*, 2016, **688**, 37-43, doi: 10.1016/j.jallcom.2016.07.167.
[28] C. H. Huang, Y. T. Yang, R. A. Doong, *Microporous and Mesoporous Materials*, 2011, **142**, 473-480, doi: 10.1016/j.micromeso.2010.12.038.
[29] J. Shi, X. Wang, *Crystal Growth & Design*, 2011, **11**, 949-954, doi: 10.1021/cg200140k.
[30] L. Meng, T. Ren, C. Li, *Applied Surface Science*, 2010, **256**, 3676-3682, doi: 10.1016/j.apsusc.2009.12.169.
[31] S. Komarneni, *Current Science*, 2003, **85**, 1730-1734.
[32] M. Shandilya, R. Rai, J. Singh, *Advances in Applied Ceramics*, 2016, **115**, 354-376, doi: 10.1080/17436753.2016.1157131.
[33] J. Zhao, W. Xing, Y. Li, K. Lu, *Materials Letters*, 2015, **145**, 332-335, doi: 10.1016/j.matlet.2015.01.049.
[34] X. Wu, S. Yin, Q. Dong, C. Guo, H. Li, T. Kimura, T. Sato, *Applied Catalysis B: Environmental*, 2013, **142-143**, 450-457, doi: 10.1016/j.apcatb.2013.05.052.
[35] R. Thapa, S. Maiti, T. H. Rana, U. N. Maiti, K. K. Chattopadhyay, *Journal of Molecular Catalysis A: Chemical*, 2012, **363-364**, 223-229, doi: 10.1016/j.molcata.2012.06.013.
[36] B. Xue, R. Liu, Z. D. Xu, *Materials Letters*, 2009, **63**, 2377-2380, doi: 10.1016/j.matlet.2009.08.023.
[37] B. Babu, A. N. Kadam, R. V. S. S. N. Ravikumar, C. Byon, *Journal of Alloys and Compounds*, 2017, **703**, 330-336, doi: 10.1016/j.jallcom.2017.01.311.
[38] A. B. Lavand, M. N. Bhatu, Y. S. Malghe, *Journal of Materials Research and Technology*, 2019, **8**, 299-308, doi: 10.1016/j.jmrt.2017.05.019.
[39] Y. Lei, L. D. Zhang, G. W. Meng, G. H. Li, X. Y. Zhang, C. H. Liang, W. Chen, S. X. Wang, *Applied Physics Letters*, 2001, **78**, 1125-1127, doi: 10.1063/1.1350959.
[40] C. Hou, B. Hu, J. Zhu, *Catalysts*, 2018, **8**, 575, doi: 10.3390/catal8120575.
[41] K. Nagaveni, M. S. Hegde, G. Madras, *The Journal of Physical Chemistry B*, 2004, **108**, 20204-20212, doi: 10.1021/jp047917v.
[42] S. N. Jamble, K. P. Ghoderao, R. B. Kale, *Journal of Physics and Chemistry of Solids*, 2018, **114**, 109-120, doi: 10.1016/j.jpcs.2017.11.012.
[43] N. Zhang, S. Ouyang, T. Kako, J. Ye, *Chemical Communications*, 2012, **48**, 9894, doi: 10.1039/c2cc34738e.
[44] C. K. Chen, S. X. Zhao, Q. L. Lu, K. Luo, X. H. Zhang, C. W. Nan, *Dalton Transactions*, 2017, **46**, 5017-5024, doi: 10.1039/c7dt00724h.
[45] K. Santhi, M. Navaneethan, S. Harish, S. Ponnusamy, C. Muthamizhchelvan, *Applied Surface Science*, 2020, **500**, 144058, doi: 10.1016/j.apsusc.2019.144058.
[46] D. Praveen Kumar, N. Lakshmana Reddy, M. Karthikeyan, N. Chinnaiah, V. Bramhaiah, V. Durga Kumari, M. V. Shankar, *Journal of Colloid and Interface Science*, 2016, **477**, 201-208, doi: 10.1016/j.jcis.2016.05.014.
[47] X. Zhou, B. Jin, J. Luo, X. Ning, L. Zhan, X. Xu, X. Fan, F. Yang, S. Zhang, *International Journal of Hydrogen Energy*, 2019, **44**, 10585-10592, doi: 10.1016/j.ijhydene.2019.02.234.

Author information

Rekha Rajput *received her M.Sc. degree in Physics (Solid State Electronics) in 2014 from The Institute of Science, Mumbai, Maharashtra, India. She is currently pursuing a Ph.D. under the guidance of Dr. Rohidas B. Kale at The Institute of Science, Mumbai. Her primary research interests include photocatalysis and photoelectrocatalysis with an emphasis on the synthesis and detailed study of the physical–chemical properties of semiconductor nanoparticles.*

Shweta Jamble *is currently an assistant professor at V. G. Vaze College (Autonomous), Mumbai. She completed each of her academic degrees from the University of Mumbai. She received her Ph.D. in physics under the guidance of Dr. Rohidas B. Kale in 2020. Her current scientific interest is mainly the synthesis, characterization of semiconductor nanomaterials and used in various applications such as photocatalysis, solar cells and optoelectronic devices.*

Dr. Rohidas B. Kale *is currently working as an Associate Professor at The Institute of science, Fort, Mumbai Maharashtra, India. He obtained his Ph.D. in 2005 from Shivaji University, Kolhapur, Maharashtra. He was a visiting scientist at National TsingHua University, Taiwan (2006-2007). He established a Thin Film Physics lab at Institute of Science. He has around 50 publications and about 1532 citations. His research is pre-eminently devoted on nanomaterials, semiconductor, luminescent materials, dye synthesized solar cell, photocatalytic materials.*

